OPEN ACCESS
IOP Publishing
Reports on Progress in Physics
Rep. Prog. Phys. **88** (2025) 048001 (15pp)
https://doi.org/10.1088/1361-6633/adc330

A mechanism for quantum-critical Planckian metal phase in high-temperature cuprate superconductors

Yung-Yeh Chang[1,2,3], **Khoe Van Nguyen**[3], **Kim Remund**[2,3] and **Chung-Hou Chung**[2,3,4,*]

[1] Institute of Physics, Academia Sinica, Taipei 11529, Taiwan
[2] Physics Division, National Center for Theoretical Sciences, Taipei 10617, Taiwan
[3] Department of Electrophysics, National Yang Ming Chiao Tung University, Hsinchu 30010, Taiwan
[4] Center for Theoretical and Computational Physics (CTCP), National Yang Ming Chiao Tung University, Hsinchu 30010, Taiwan

E-mail: chung0523@nycu.edu.tw

Received 3 October 2024, revised 19 March 2025
Accepted for publication 20 March 2025
Published 10 April 2025

Corresponding editor: Dr Paul Mabey

Abstract

The mysterious metallic phase showing T-linear resistivity and a universal scattering rate $1/\tau = \alpha_P k_B T/\hbar$ with a universal prefactor $\alpha_P \sim 1$ and logarithmic-in-temperature singular specific heat coefficient, the so-called 'Planckian metal phase' was observed in various overdoped high-T_c cuprate superconductors over a finite range in doping. Revealing the mystery of the Planckian metal state is believed to be the key to understanding the mechanism for high-T_c superconductivity. Here, we propose a generic microscopic mechanism for this state based on quantum-critical local bosonic charge Kondo fluctuations coupled to both spinon and a heavy conduction-electron Fermi surface within the heavy-fermion formulation of the slave-boson t–J model. By a controlled perturbative renormalization group analysis, we examine the competition between the pseudogap phase, characterized by Anderson's Resonating-Valence-Bond spin-liquid, and the Fermi-liquid state, modeled by the electron hopping (effective charge Kondo effect). We find a quantum-critical metallic phase with a universal Planckian $\hbar\omega/k_B T$ scaling in scattering rate near an extended localized-delocalized (pseudogap-to-Fermi liquid) charge-Kondo breakdown transition. The d-wave superconducting ground state emerges near the transition. Unprecedented qualitative and quantitative agreements are reached between our theoretical predictions and various experiments, including optical conductivity, universal doping-independent field-to-temperature scaling in magnetoresistance, specific heat coefficient, marginal Fermi-liquid spectral function observed in ARPES, and Fermi surface reconstruction observed in Hall coefficients in various overdoped cuprates.

* Author to whom any correspondence should be addressed.

Our mechanism offers a microscopic understanding of the quantum-critical Planckian metal phase observed in cuprates and its link to the pseudogap, d-wave superconducting, and Fermi liquid phases. It offers a promising route for understanding how d-wave superconductivity emerges from such a strange metal phase in cuprates–one of the long-standing open problems in condensed matter physics since 1990s–as well as shows a broader implication for the Planckian strange metal states observed in other correlated unconventional superconductors.

Supplementary material for this article is available online

Keywords: high-Tc cuprate superconductors, Planckian dissipation, strange metal, non-Fermi liquid, spin liquid, quantum phase transitions and quantum criticality, Kondo physics in heavy-fermion systems

1. Introduction

Over the past three decades, metallic behavior that cannot be described within the Fermi liquid (FL) paradigm has commonly been observed in a wide variety of strongly correlated quantum materials. Yet, the emergence of such metals is poorly understood. This non-Fermi liquid behavior often exists near a quantum phase transition, and shows 'strange metal (SM)' phenomena with (quasi-)linear-in-temperature decreasing resistivity and divergent logarithmic-in-temperature specific heat coefficient as $T \to 0$.

One particularly intriguing class of SM states is the 'Planckian metal', observed in the normal state of unconventional superconductors, including cuprate superconductors [1–3], iron pnictides and chalcogenides [4–8], organic [9, 10] and heavy-fermion compounds [10–13], and twisted bilayer graphene [14]. It shows perfect T-linear scattering rate, reaching 'Planckian dissipation limit' allowed by quantum mechanics, $1/\tau(T) = \alpha_P k_B T/\hbar$ with $\alpha_P \sim 1$. This generic and mysterious phenomenon deserves further theoretical study. Here, we focus on the Planckian metal physics in high-T_c cuprates. In cuprates, d-wave superconductivity (dSC) emerges out of this exotic state of matter with decreasing temperatures, it was argued that revealing the mystery of the Planckian metal state is the key to understanding the mechanism for high-T_c superconductivity in cuprates [15, 16]. Experimental observations in heavy-fermion superconductors suggest that α is a non-universal constant but depends on the strength of the Kondo correlations [17]. By contrast, in overdoped cuprates the Planckian perfect T-linear scattering rate with the same α persists from very high temperatures ($T \sim 300$ K) to very low temperatures ($T \to 0$) over a wide range of samples near optimal doping, indicating that the Planckian state in overdoped cuprates might be a universal feature. The Planckian behavior across the entire temperature range, in particular for the low temperature regime ($T \to 0$) in cuprates, is unlikely to be explained by phonons whose contributions are mainly at high temperatures, even though electron-phonon coupling is also known to give rise to T-linear resistivity in normal metals [18]. Note that if phonons were to significantly contribute to the linear-T resistivity in cuprates, one would expect the slope to deviate at a certain characteristic temperature as phonon scattering becomes significant with increasing temperature. However, no such slope change is clearly observed experimentally [19], indicating that the contribution from phonons to T-linear resistivity is negligible. Meanwhile, frequency-to-temperature ($\hbar\omega/k_B T$) scaling from optical conductivity measurement [20] and field-to-temperature (B/T) scaling in magnetoresistance as well as other quantum critical-like properties extending over a range from the critical doping to the end of the dSC dome in various hole-doped [21] and electron-doped [22, 23] cuprates strongly suggest that a Planckian state is a quantum critical 'phase' [16]. These observations lead to fundamental questions: What is the microscopic mechanism for this exotic phase of matter and its links to quantum criticality and the neighboring phases? The Planckian metal state lies in between the pseudogap and FL phases with localized and itinerant characters of electrons, respectively. This points to an appealing scenario in which the Planckian metal phase may arise near a possible localized-delocalized quantum critical point due to competition between the pseudogap and FL phases, and the dSC is reached by condensing this quantum critical metal.

It is challenging to develop a controlled approach for this exotic state of matter. Recently, this state has been realized theoretically via controlled large-N approach of the t-J model with random hopping and exchange couplings, the 'SYK model' [24–26] and in the Hubbard model by Quantum Monte Carlo [27]. Nevertheless, a microscopic understanding of this state in terms of critical spin and charge fluctuations within the well-established non-random Hubbard or t–J model framework has yet to be developed.

In this work, we address the microscopic mechanism for the Planckian metal phase in cuprates via different approaches from the previous ones [28–31] based on recently developed heavy-fermion perspective of the two-dimensional slave-boson t-J model, known to offer qualitative understanding of cuprate phase diagram, in the formulation of the Kondo–Heisenberg lattice model [32]. Within our framework, the Kondo–Heisenberg slave–boson (KHSB) t–J model, the Planckian metal phase appears as a result of local disordered bosonic charge fluctuations coupled to a fermionic spinon band and a heavy-electron band near a localized–deloclaized quantum critical point due to the competition between the pseudogap and FL phases. In this approach, the hopping of electrons is expressed in terms of effective Kondo

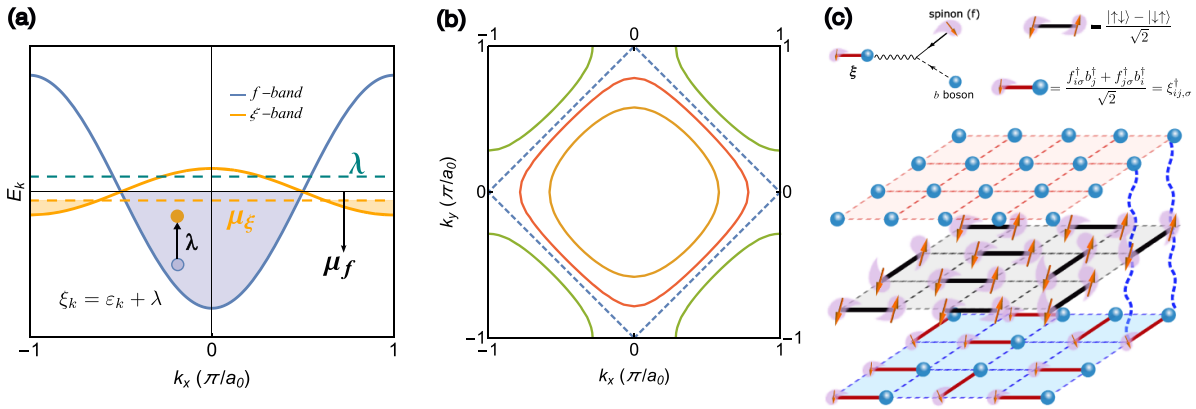

Figure 1. (a) Schematic plots for the dispersive f-spinon (blue curve) and the weakly dispersive ξ (orange curve) bands (corresponding to hole doping δ), associated with their chemical potentials, μ_f and μ_ξ. The green dashed line denotes the energy level (Lagrange multiplier) λ for the slave boson. The shaded areas represent filling of the f- and ξ-bands. a_0 here denotes the lattice constant. (b) Fermi surfaces of the f-spinon band (blue) and of the ξ band with different levels of hole doping (orange for hole doping δ, green for $1+\delta$, and red in between δ and $1+\delta$). (c) Main plot: Schematic plot of strange-metal state. The blue dashed curves represent the Kondo-like hopping term. Upper left: Feynman diagram for the interaction vertex of the Kondo-like hopping term. Upper right: the RVB spin-singlet bond in the f-spinon band and the spinon-holon bound state (the ξ field).

hybridization between a composite fermionic spinon-holon bound state representing conduction band and a charge-neutral gapless fermionic spinon band with a Fermi surface (see figure 1 (a) and (b)), while as the Heisenberg exchange coupling is described by resonating-valence-bond (RVB) spin-liquid with both hopping of fermionic spinons and singlet pairing between them. The mean-field theory of this approach captures qualitatively the pseudogap, FL, and d-wave superconducting phases. In particular, it advances the previous slave-boson t–J approach by capturing aspects of coherent quasi-particle excitation observed at nodal Fermi pocket in the pseudogap phase. Meanwhile, the spin-liquid state here is further stabilized by coupling to charge Kondo hybridization, similar to the Kondo-stabilized spin-liquid mechanism in heavy-fermion systems [33]. Here, by perturbative renormalization group analysis, we study the quantum phase transition of the model beyond mean-field and seek the possible emergence of Planckian metal state due to spin and charge fluctuations near criticality. Our approach is highly motivated by the striking similarity in SM phenomenology between cuprates [21, 34] and heavy-fermion Kondo lattice systems [35, 36], in which the Fermi surface volume reconstructs over the entire SM region in both systems. This indicates a Kondo-breakdown-like physics observed in heavy-fermion systems may appear in cuprates where the SM state and Fermi surface reconstruction occur simultaneously near the Kondo breakdown QCP due to coupling of local charge fluctuations to the Fermi surface [17, 37, 38]. A related yet distinct heavy-fermion Kondo lattice approach was proposed in [39] to address the evolution from the pseudogap metal with small Fermi surfaces to the conventional FL with a large Fermi surface.

Via the controlled RG analysis, a stable quantum critical Planckian SM phase over a finite range in doping with universal T-linear scattering rate ($\alpha \sim O(1)$ being a universal constant independent of microscopic couplings) is realized near a localized–delocalized Kondo breakdown transition. Therein, the local bosonic charge (effective Kondo) fluctuations coupled to composite fermionic conduction band and gapless fermionic spinons (see figure 1(c)). The universal quantum critical ω/T-scaling is found in this phase in dynamical scattering rate, in excellent agreement without fine-tuning with the optical conductivity measurement [20], and the universal doping-independent field-to-temperature scaling in magnetoresistance over an extended doping range in [21] in the SM region of various overdoped cuprates. The marginal FL single-electron spectral function and crossover in Fermi surface volume in this phase are both in excellent agreement with ARPES [40] and Hall measurements [21, 34], respectively. Our results in thermodynamic properties near the transition well captures the power-law singularity in specific heat coefficient observed in a class of cuprates near pseudogap end point [34, 41]. Our study indicates that this exotic phase is a quantum critical phase governed by the critical charge (effective Kondo) fluctuations at the localized–delocalized Kondo breakdown quantum critical point arising from the competition between the pseudogap (Cooper-pair formation) and FL (electron hopping) phases. It provides a coherent understanding of the quantum-critical SM state within the context of the global phase diagram of cuprate superconductors and reconciles the seemingly inconsistent scenarios of the SM state observed in cuprates. Our mechanism offers a promising route for understanding how dSC emerges from such a SM phase in cuprates–one of the long-standing open problems in condensed matter physics since 1990s. It shows a broader implication for the universal Planckian SM states observed in other correlated unconventional superconductors.

2. Results

Before presenting our model Hamiltonian, we would like to make general remarks on the applicability of the t–J model for cuprtaes. The simple one-band 2D Hubbard model has

been considered as an appropriate 'minimum parent' model to qualitatively capture the key features of high-T_c cuprates [42], including the anti-ferromagnetic Mott insulating state at half-filling, the d-wave superconducting dome in the intermediate doping range, the pseudogap phase (charge-density-wave and spin-density-wave states) in underdoped region, FL on the overdoped side, and the SM state near optimal doping [27]. In the strongly correlated limit where $t/U \ll 1$, the Hubbard model is effectively reduce to the t–J model [43]. The t–J model has been extensively used as an effective model for describing cuprates (see for example [44]). This is justified since typical cuprates fall into the strongly correlated regime with very small t/U ($t \sim 0.4$ eV, $U \sim 5-10$ eV, $t/U \sim 0.04-0.08$) [44]. The t–J model studied by various analytical and numerical methods has been shown to provide qualitative and some quantitative understanding of important aspects of cuprates phenomena, including: doping vs. temperature phase diagram, the d-wave superconducting dome, the pseudogap (d-wave superconducting) phase in terms of phase incoherent (phase coherent) RVB Cooper pair, respectively, various broken symmetry states and Fermi-arc observed in the pseudogap phase [32, 44, 45]. It therefore serves as a simplified yet an appropriate model for cuprates. Whether the t–J model can be extended to describe other materials showing similar Planckian metal behaviors, or whether there exists a single microscopic mechanism that unifies the understanding of the similar Planckian metal states across different materials is an outstanding open problem, which deserves further study elsewhere.

2.1. Heavy-fermion formulation of the slave-boson t–J model

We start from the Hamiltonian of the slave-boson representation of t-J model on a 2D lattice [32], describing as $H = H_t + H_J$ with $H_t = -t\sum_{\langle i,j\rangle,\sigma} c^\dagger_{i\sigma}c_{j\sigma} - \mu\sum_{i\sigma} c^\dagger_{i\sigma}c_{i\sigma}$ and $H_J = J_H\sum_{\langle i,j\rangle} \boldsymbol{S_i}\cdot\boldsymbol{S_j}$. Here, (t, μ, J_H) denotes the (hopping strength, chemical potential, Heisenberg coupling), and $\langle i,j\rangle$ the nearest-neighboring sites, and the local spin operator $\boldsymbol{S}_i = \frac{1}{2}\sum_{\sigma\sigma'} c^\dagger_{i\sigma}\boldsymbol{\sigma}_{\sigma\sigma'}c_{i\sigma'}$. Under the slave-boson representation $c^\dagger_{i\sigma} \to f^\dagger_{i\sigma}b_i$ with $f_{i\sigma}\,(b_i)$ being fermionic charged-neutral spinon (bosonic spinless charged holon), we further factorize the H_t and H_J terms via Hubbard-Stratonovich transformation following [32], i.e. $H_t \to t\sum_{\langle i,j\rangle,\sigma}\left[\left(f^\dagger_{i\sigma}b^\dagger_j + f^\dagger_{j\sigma}b^\dagger_i\right)\xi_{ij,\sigma} + H.c.\right]$ and $H_J \to \sum_{\langle i,j\rangle\sigma}\left(-\chi_{ij}f^\dagger_{i\sigma}f_{j\sigma} + \Delta_{ij}\tilde{\sigma}f^\dagger_{i\sigma}f^\dagger_{j,-\sigma} + H.c.\right)$, $\tilde{\sigma} \equiv \mathrm{sgn}(\sigma)$.

Note that we decompose the Heisenberg interaction into both the particle-hole and particle-particle forms. Here, $\xi_{ij,\sigma}$, χ_{ij}, and Δ_{ij} represent the auxiliary Hubbard–Stratonovich fields living between sites i and j, as a result, their degrees of freedom for the bond fields are twice as many as that for b and f. The χ_{ij} and Δ_{ij} fields represent the spinon hopping and pairing bond fields, respectively, whose condensate play the role of the effective hopping and pre-formed singlet d-wave Cooper pairing of spinons in the RVB spin liquid. The model shows a U(1) gauge symmetry: $f_{i\sigma} \to f_{i\sigma}e^{i\theta_i}$, $b_i \to b_i e^{i\theta_i}$, $\chi_{ij} \to \chi_{ij}e^{i(\theta_i-\theta_j)}$ and $\xi_{ij,\sigma} \to \xi_{ij,\sigma}e^{i(\theta_i+\theta_j)}$, hence the Ward identity is expected to be satisfied. A finite and uniform mean-field $\chi = \langle\chi_{ij}\rangle$ is assumed. The $\xi_{ij,\sigma}$ field, previously proposed in [32, 46, 47], describes a gauge charge-$2e$ spinon-chargeon bound state; it further advances the original slave-boson approach by capturing the nodal Fermi pocket (arc) quasi-particle excitations in the pesudogap phase of cuprates. The hopping term H_t, after the decomposition, behaves as an effective Kondo coupling in the charge sector. If the slave boson b gets Bose condensed, the ξ fermion becomes a physical conduction electron. Terms containing slave boson occupation number n^i_b are neglected in the Hubbard–Stratonovich transformation for H_t and H_J. The constraints $b^\dagger_i b_i + \sum_\sigma f^\dagger_{i\sigma}f_{i\sigma} = 1$ is imposed [32, 48, 49]. Four distinct mean-field phases are realized in this model, depending on whether or not the two boson fields b and Δ get Bose-condensed (see figure 3(b) and [32]): the pseudogap phase, known as Z_2 fractionalized FL or Z_2 FL*, (Landau Fermi liquid, FL) is reached when $\Delta \neq 0, \langle b\rangle = 0\,(\Delta = 0, \langle b\rangle \neq 0)$; while the U(1) FL* ($d$-wave superconducting) phase arises when $\langle b\rangle = \Delta = 0\,(\langle b\rangle \neq 0, \Delta \neq 0)$. The Z_2 FL* and U(1) FL* phases realized here are examples of the previously proposed fractionalized FL states in [50] in the context of heavy-fermion Kondo lattice systems with a small Fermi surface volume and charge-neutral fractionalized spinon excitations which carry a gauge charge characterizing the topological order. The spinons in these two fractionalized spin-liquid phases are deconfined due to the existence of a spinon Fermi surface, and are thus stable against U(1) gauge field fluctuations [51, 52]. Meanwhile, these two fractionalized phases are energetically more stable compared to that in the earlier approach of slave-boson t–J model [49] by the charge Kondo hybridization term, similar to the Kondo-stabilized spin-liquid mechanism in heavy-fermion systems [33, 53].

We shall explore the phase diagram in U(1) FL* phase beyond mean-field by including fluctuations of both t- and J-terms. We will not include U(1) gauge fluctuations in our RG analysis since the spinons are deconfined and stable against them due to the presence of a spinon Fermi surface [51]. The leading effective action in units of the half-bandwidth of the f–spinon band $D \approx 4\chi \approx 4J_H$ beyond the mean-field level reads ($\hbar = k_B = 1$) [32]

$$\begin{aligned} S = &-\sum_{k\sigma} f^\dagger_{k\sigma}\mathcal{G}_f^{-1}(k)f_{k\sigma} - \sum_k b^\dagger_k\mathcal{G}_b^{-1}(k)b_k \\ &+ \sum_{k\sigma a}\xi^{a\,\dagger}_{k\sigma}\mathcal{G}_\xi^{-1}(k)\xi^a_{k\sigma} + \sum_{ka}\varphi^{a\,\dagger}_k\mathcal{G}_\varphi^{-1}(k)\varphi^a_k \\ &+ \frac{g}{\sqrt{\beta N_s}}\sum_{kp\sigma a}\left(f^\dagger_{k\sigma}b^\dagger_p\xi^a_{k+p,\sigma} + H.c.\right) \\ &+ \frac{J}{\sqrt{\beta N_s}}\sum_{kpa}\left[f^\dagger_{k\uparrow}f^\dagger_{p\downarrow}\varphi^a_{k+p} + H.c.\right] \end{aligned} \tag{1}$$

with $k = (\boldsymbol{k}, \omega)$ and $p = (\boldsymbol{p}, \nu)$, φ being the fluctuating field for the d-wave RVB pairing order parameter Δ. In the phases with $\langle b\rangle = 0$, the bare hopping parameter t is strongly suppressed by the disordered bosons, leading to an effective hopping $g \equiv 2t\sqrt{\delta}$. Here, $J = 2J_H$ is the effective exchange, $\mathcal{G}_f(k) = (i\omega - \varepsilon_{\boldsymbol{k}})^{-1}$, $\mathcal{G}_\xi(k) = \zeta^{-1}(i\omega - \xi_{\boldsymbol{k}})^{-1}$, $\mathcal{G}_b = (i\omega - \lambda)^{-1}$, and $\mathcal{G}_\varphi =$

$(J/2)^{-1}$ denote the bare Green's functions (see appendix B). The momenta relevant for the bosonic φ field are near the antinode. Our perturbative expansion in bare couplings g, J is controlled since $g/D, J/D < 1$ (for an estimated $J_H/t \sim 0.3$). To study the charge dynamics and transport properties, we go beyond static mean-field level of ξ field by generating its dynamics and dispersion via second-order hopping process at fixed $g = g_0^*$ such that $\zeta^{-1} \equiv (g^2\rho_0/D)^{-1}$ appears as a prefactor in $\mathcal{G}_\xi$, with $\rho_0 = 1/D$ being the constant density of states at Fermi level for f spinon band. The f-spinon band is approximated by a linear-in-momentum dispersion, namely $\varepsilon_{\boldsymbol{k}} = h_{\boldsymbol{k}} - \mu_f \approx v|\boldsymbol{k}|$ with $h_{\boldsymbol{k}} \equiv -2\chi(\cos k_x + \cos k_y)$ and $\mu_f = \mu - \lambda$ being the effective chemical potential for f spinon (μ is the chemical potential for the original conduction electron, see appendix A). Here, the spinon band is fixed at half-filling, $\mu_f = 0$. The band structure for the ξ fermion shows a hole-like dispersion, $\xi_{\boldsymbol{k}} = -\zeta\varepsilon_{\boldsymbol{k}} - \mu_\xi$. The Lagrange multiplier $\lambda > 0$ is introduced to enforce the local constraint for slave boson. The slave boson (b field) is effectively treated as a local boson with a flat band of energy λ and with a negligible dispersive band (see appendix B). In the pseudogap and U(1) FL* phases, the chemical potential of the ξ band μ_ξ fixes hole doping δ for the system such that $N_s^{-1}\sum_{ij,\sigma}\langle\xi^\dagger_{ij,\sigma}\xi_{ij,\sigma}\rangle = \delta$. Note that equation (1) is also applicable when d-wave preformed Cooper pair order, relevant for temperatures slightly above the superconducting transition temperature of cuprates, is replaced by the pair density wave state, considered as a hallmark of pseudogap phase at higher temperatures [54, 55].

2.2. Renormalization group analysis

The perturbative RG analysis is applied to the effective action of the modified slave-boson model equation (1) by considering the one-loop diagrams shown in figure 2. It is convenient to define the dimensionless bare coupling constants $g \to g/D$, $J \to J/D$, and absorb $1/\zeta$ in $\mathcal{G}_\xi$ into g by a rescaling, $g \to \bar{g} = g/\sqrt{\zeta}, \xi \to \sqrt{\zeta}\xi$. Our RG analysis is perturbatively controlled as $\bar{g} < 1$ (the bare value $g < g_0^*$ is set), and $J < 1$. Our RG approach can be further controlled by the ϵ-expansion technique with a small parameter $\epsilon = d - z$ within the convergence radius $|\epsilon| \leqslant 1$. We set the dynamical exponent $z = 1$ due to the linearized dispersion of f, and spatial dimension $d = 2$ here. The RG scaling equations of the running renormalized dimensionless couplings, $\bar{g}(\ell)\rho_0$ and $J(\ell)\rho_0$ read (see appendix C)

$$\begin{aligned}\frac{\mathrm{d}\left(\bar{g}\left(\ell\right)\rho_0\right)}{\mathrm{d}\ell} &= -\left(\frac{\epsilon}{2}\right)\left(\bar{g}\left(\ell\right)\rho_0\right) + \left(\bar{g}\left(\ell\right)\rho_0\right)^3,\\ \frac{\mathrm{d}\left(J\left(\ell\right)\rho_0\right)}{\mathrm{d}\ell} &= -\left(\frac{\epsilon}{2}\right)\left(J\left(\ell\right)\rho_0\right) + \left(J\left(\ell\right)\rho_0\right)\left(\bar{g}\left(\ell\right)\rho_0\right)^2\\ &\quad + \frac{3}{2}\left(J\left(\ell\right)\rho_0\right)^3, \end{aligned} \tag{2}$$

where scaling parameter $\ell \equiv -\ln D > 0$. The RG flow equations of equation (2) is shown in figure 3(a) where the critical fixed point occurs at $C_r = (J^*\rho_0, \bar{g}^*\rho_0) = (\sqrt{\epsilon/2}, \sqrt{\epsilon/3})$. For simplicity, the U(1) gauge-field fluctuations are not included in our RG analysis; nevertheless, its effect on transport and thermodynamic properties are addressed in Discussions (see also appendix E1).

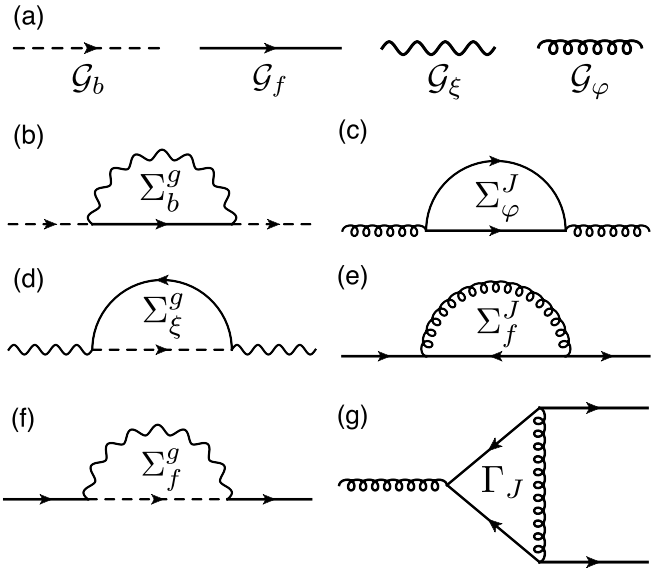

Figure 2. The Feynman diagrams for the self-energy and vertex correction being used in the RG analysis. (a) The graphical representation of the bare propagator of various fields/operators. Feynman diagrams of the (b)–(f) self-energy and (g) vertex correction for H_J.

RG flow and phase diagram. As shown in figure 3(a), our one-loop RG flow diagram supports a quantum critical point (QCP) at C_r, separating the four phases: the pseudogap PSG (FL) phase is reached when the Heisenberg coupling J becomes relevant (irrelevant), while the hopping (effective Kondo) term $\bar{g}$ becomes irrelevant (relevant); the d-wave superconducting state (U(1) FL*, SM) phase arises for both $\bar{g}$ and J being relevant (irrelevant), respectively. Near C_r, the correlation length $\eta(\ell)$ shows a power-law divergence as: $\eta(\ell) \sim \ell^{-\nu}$ with the exponent $\nu = 1$, indicating linear-in-doping crossover scales $T^*, T_{\mathrm{FL}} \propto \eta^{-z} \propto |\delta - \delta_c|$, corresponding to the PSG→SM and SM → FL crossovers, respectively [56]. We shall see below that the systems with initial couplings flowing to the mean-field U(1) FL* fixed point show SM features with universal quantum critical Planckian scaling in electron scattering rate; therefore beyond mean-field under RG, it corresponds to the SM fixed point.

2.3. Physical observables near the QCP

To highlight the significance of our results and make a clear comparison of our results to the experiments, before we present our results, we would like to briefly summarize the key experiments and discuss the corresponding debated issues on the SM state of high-T_c cuprates in literature both in transport and thermodynamic properties.

First, the perfect T-linear resistivity over a wide range in temperature has been a hallmark of SM state in normal state of high-T_c cuprates close to optimal doping since its discovery in late 1980s' [57–59]. Early experimental studies suggested the funnel-shaped SM normal state as a function of

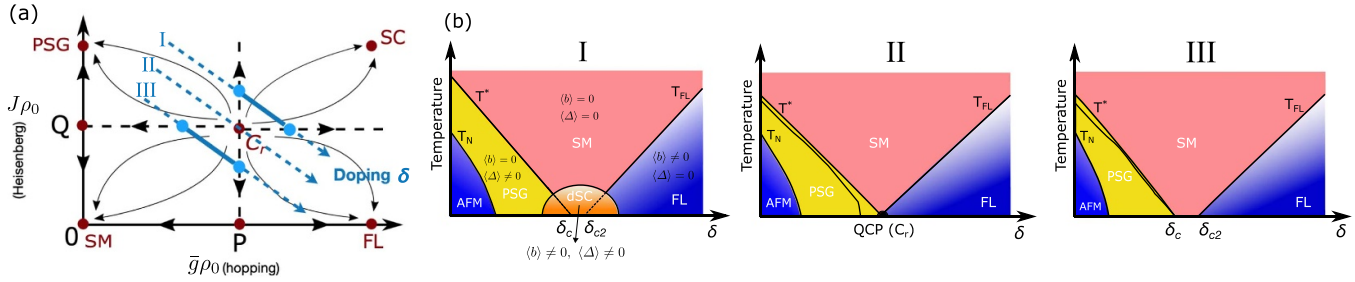

Figure 3. (a) Plot of the RG flow for the Heisenberg and hopping terms. Paths I, II, III in (a) indicate the three types of phase diagram that can be accessed from the RG equations. (b): three possible distinct types of phase diagrams (I, II, III) corresponding to paths (I, II, III) from the RG flow diagram in (a). $T_{\rm N}$, T^*, and $T_{\rm FL}$ denote the temperature crossovers for the anti-ferromagnetic order, pseudogap, and FL states, respectively. In (b)-I, δ_c and δ_{c2} represent the critical points associated respectively with PSG-SM and SM-FL transitions once superconductivity is suppressed.

temperature and doping is expected to end at a hidden QCP inside the superconducting dome [60]. However, more recent studies on different cuprate compounds revealed an extended SM phase ranging from slightly under-doped to over-doped region when superconductivity is suppressed by a large magnetic field [21, 34]. One important debate is: whether the SM state with T-linear resistivity is considered as a quantum critical state due to the hidden QCP or it is a entirely new phase of matter over an extended doping range, which might not be related to quantum criticality? Our study offers a unified framework to reconcile these two seemingly inconsistent pictures.

A more exotic and intriguing property of SM state with T-linear resistivity in cuprates (as well as in other correlated unconventional superconductors) is that by analyzing the DC-resistivity it shows a universal Planckian scattering rate, see, for example [2, 10]. It was argued in [15] that the reason why the d-wave superconducting transition temperature $T_{\rm c}$ is so high in cuprates is due to the fact the normal state of it is a Planckian metal with a scattering rate reaching the Planckian dissipation limit–the maximum dissipation allowed by quantum mechanics. To reach this Planckian limit, the author in [15] further proposed that the quantum system has to be quantum critical. A key debated issue is: what is the possible microscopic origin of the proposed quantum criticality if it exists at all? Experimentally, to extract the scattering rate from DC-resistivity and show that it is Planckian relies on the DC-Drude formula $\rho(T) = \frac{m^*}{ne^2}\frac{1}{\tau(T)}$ with the effective mass m^* estimated independently from specific heat [2] or quantum oscillation experiments [61] , and where n is the charge carrier density $n = \frac{1-\delta}{V}$ [2], where V is the unit cell volume [2] (and where n/m^* is assumed to be temperature independent). However, this approach–by combing different experimental measurements in the same equation–may reduce the quantitative accuracy in determining the Planckian coefficient α since the estimated value for m^* via specific heat measurement may quantitatively differ from that via quantum oscillation experiment.

By contrast, a more quantitatively accurate and consistent experimental approach to obtain the Planckian scattering rate is via AC-conductivity measurement as shown in [20, 62] for heavy-fermion compounds. Indeed, one can probe the scattering rate $\frac{1}{\tau(\omega,T)}$ and the effective mass m^* simultaneously by considering the AC conductivity [20, 62]. This is easily noticed by considering the generalized AC drude formula for the conductivity that accounts for the mass enhancement $\frac{m^*(\omega)}{m}$ [20]:

$$\sigma(\omega,T) = \frac{\frac{e^2K}{\hbar^2 d_{\rm c}}}{\frac{1}{\tau(\omega,T)} - i\omega\frac{m^*(\omega,T)}{m}}\,, \tag{3}$$

where $d_{\rm c}$ is distance between two CuO_2 planes and K is the spectral weight for a single plane $K = \frac{\hbar^2 d_{\rm c}}{e^2}\phi(0)$, with $\phi(\epsilon) = 2\frac{e^2}{\hbar^2}\int_{BZ}\frac{{\rm d}^2k}{(2\pi)^2}(\frac{{\rm d}\epsilon_{\mathbf{k}}}{{\rm d}k_x})^2$ [20], such that K is a function of the ration $\frac{n}{m^*}$ and is also assumed to be temperature independent. The two unknown parameters being the the scattering rate $\frac{1}{\tau(\omega,T)}$ and the effective mass $\frac{m^*(\omega,T)}{m}$ can be deduced simultaneously by considering both the real and the imaginary part the conductivity [20]:

$$\frac{1}{\tau(\omega,T)} = \frac{e^2K}{\hbar^2 d_{\rm c}}{\rm Re}\left[\frac{1}{\sigma(\omega,T)}\right]\,, \tag{4}$$

$$\frac{m^*(\omega,T)}{m} = \frac{e^2K}{\hbar^2 d_{\rm c}}{\rm Im}\left[\frac{1}{\omega\sigma(\omega,T)}\right]\,. \tag{5}$$

Second, ARPES is a direct transport probe to local single-particle spectral function. Since 1999, there has been experimental reports via ARPES [63–65] on the Marginal Fermi Liquid (MFL) behavior proposed in [66] in the SM state of cuprates with the following self-energy:

$$\Sigma(\mathbf{k},\omega) = \Sigma'(\mathbf{k},\omega) + i\Sigma''(\mathbf{k},\omega) = \lambda\left[\omega\log\left(\frac{x}{\omega_c}\right) - i\frac{\pi}{2}x\right] \tag{6}$$

where $x = \max(|\omega|,T)$ [66]. The similar MFL behavior has also been observed in more recent ARPES studies on the SM state of cuprate [40]. The significances of these results are: (i) The quasi-particle weight $z = 1/(1-\frac{{\rm d}\Sigma'}{{\rm d}\omega}) \to 0$ as $\frac{1}{\log(\omega)}$ at the Fermi surface, indicating the breakdown of the FL picture (with a finite z); (ii) The single-particle scattering rate Σ'' is proportional to $x \approx \max(|\omega|,T)$; and the leading order

contribution to Σ'' is independent of momentum both perpendicular to and around the Fermi surface, indicating a 'local' self-energy; (iii) The combination of momentum independence of self-energy and the linear dependence on x of Σ'' in the MFL form of the self energy, equation (6), leads to a resistivity that is linear in T. However, the microscopic theory of MFL and its link to universal Planckian scattering rate, as well as possible local quantum criticality near optimal doping is still an open problem [67]. Our theoretical framework provides a mechanism for this universal MFL state.

Finally, the T-logarithmic enhancement of specific heat coefficient (or γ-coefficient) upon decreasing temperature is another hallmark of SM state in cuprtaes [34, 41, 67]:

$$\frac{C_{el}}{k_{\rm B}T} = \gamma\left[1+\tilde{g}\ln\left(\frac{T_x}{T}\right)\right], \tag{7}$$

where $\tilde{g}$ is some coupling constant and T_x is a cutoff scale. Such singular behavior in γ-coefficient can be accounted for within the MFL proposal in [66, 67] as well as within our theoretical framework (see below). Interestingly, the value of γ in low temperature limit has been reported to show a rapid increase as doping approaches a critical value $\delta^* \simeq 0.19$ [34, 41]. However, whether this rapid increase in γ is a signature of quantum criticality with a power-law divergence ($\gamma \simeq (\delta-\delta^*)^{-m}$) [41, 67, 68] or it is not a true divergence but a finite enhancement due to the Lifshitz transition where the Fermi surface changes from a hole–like to an electron–like band structure [69] is still under debate. We find that our charge-Kondo-breakdown scenario within the heavy-fermion slave-boson t–J model supports a power–law singular $\gamma(T\to 0)$ near the QCP with the divergent power-law exponent $m \simeq 0.5$, in agreement with the results shown in [41] and [34]. Below we present our results in details.

2.3.1. Conductivity and scattering rate. The total conductivity $\sigma_{\rm tot} = \rho_{\rm tot}^{-1}$ can be computed via the rule by Ioffe and Larkin [70]: $\sigma_{\rm tot} = \sigma_\xi\sigma_f/(4\sigma_\xi+\sigma_f)$. Because the slave boson is localized and has negligible dispersion, it does not contribute to the conductivity. Since the effective mass of the ξ band is much heavier than that for the f spinons, $m_\xi/m_f \sim 1/\zeta \gg 1$, resistivity is dominated by the ξ-band, leading to $\rho_{\rm tot} = 1/\sigma_{\rm tot} \approx 1/\sigma_\xi = \rho_\xi$. In the theory of local (momentum independent) self-energy, the vertex corrections are negligible, and the optical conductivity can be obtained directly from the self-energy, $\sigma(\omega) = (i\Phi(0)/\omega)\int_{-\infty}^{\infty} {\rm d}\varepsilon\,[n_{\rm F}(\varepsilon) - n_{\rm F}(\varepsilon+\hbar\omega)]/[\hbar\omega + \Sigma_c^*(\varepsilon) - \Sigma_c(\varepsilon+\hbar\omega)]$, where $\Phi(\varepsilon)$ is the transport function (see [20] for details). Therefore, electron transport time is equivalent to the relaxation time since $\sigma_{\rm tot} \sim \sigma_\xi$. The total scattering rate is hence dominated by the contribution from the ξ field: $1/\tau_{\rm tot} \sim 1/\tau_\xi$. In the SM state with $\langle b\rangle = \Delta = 0$, the gauge-invariant (physical) electron operator can be constructed from ξ_{ij} and φ_{ij} as $c = \xi\sqrt{2}\varphi_{ij}^*\sqrt{J}$. The dynamical scattering (relaxation) rate at $T=0$ is calculated via the imaginary part of the electron self-energy: $\tau(\omega) = -\hbar/2\Sigma_c''(\omega)$ and $\Sigma_c''(\omega) = (1/2)\Sigma_\xi''(\omega)$, where $\Sigma_\xi''(\omega)$ at $T=0$ is obtained via second-order RG renormalized perturbation close to the QCP with bare couplings being replaced by the renormalized ones i.e. $\bar{g}, \bar{g}_0^* \to \bar{g}(\ell)$, showing a universal local MFL self-energy insensitive to couplings [71], including a constant and a linear-in-$|\omega|$ term, i.e. $\Sigma_\xi''(\omega) = \alpha - \varsigma\,|\omega|$ with $\alpha \approx \frac{5}{2}\bar{g}^2\rho_0 = \frac{5}{2}D$ and $\varsigma = \frac{2}{\pi}$. This local self-energy Σ_ξ comes as a consequence of the local nature of the slave boson in our approach. The constant α is generated by the fluctuating non-condensed local slave-bosons through self-energy of the ξ field, reminiscent of electrons in metals being scattered by disordered random impurities.

2.3.2. Quantum critical phase with universal Planckian scattering rate. Close to the QCP in the scaling regime where conformal symmetry is present, the scattering rate at finite temperatures can be derived from the scattering rate $T=0$, $1/\tau(\omega, T=0)$, by a conformal transformation [20, 73, 74]. Strikingly, following path III of figure 2(a) over the region where both $\bar{g}(\ell)$ and $J(\ell)$ are irrelevant, we discover a quantum critical Planckian SM 'phase' with universal quantum-critical ω/T-scaling in the scattering rate that is independent of coupling constant (see Appendices E1 and F):

$$\frac{1}{\tau(x)} - \frac{1}{\tau_0} = \frac{4}{\pi}k_{\rm B}Tf\left(\frac{x}{2}\right), f\left(\frac{x}{2}\right) = \frac{x}{2}\coth\left(\frac{x}{4}\right) \tag{8}$$

with $x \equiv \hbar\omega/k_{\rm B}T$ and $\tau_0 \equiv \tau(\omega=0, T=0)$. Surprisingly, as shown in figure 4(a), the universal Planckian scattering rate of equation (8) is in excellent agreement with the recent optical conductivity measurement in [20] without fine-tuning. Note that the experimental data on optical conductivity shown in figures 4(a)and (b) do not cleanly collapse into a single curve at low frequency [20], possibly due to enhanced low-frequency noise or the presence of some small mass in the scattering mediator. In the high-frequency, low-temperature limit $x \gg 1$, the scattering rate divided by $k_{\rm B}T$ shows a universal scaling behavior, $\frac{\tau^{-1}(T)}{k_{\rm B}T} \approx (2/\pi)x$. Conversely, in the DC-limit ($x\to 0$), the scattering rate manifests the Planckian scattering rate, revealing a universal feature that is insensitive to microscopic coupling constants: $1/\tau \approx \alpha_P k_{\rm B}T/\hbar$ with $\alpha_P \approx 8/\pi$, in reasonably good agreement with DC-scattering rate estimated in various overdoped cuprates [2, 20]. We find that this universal feature of the scattering rate, which is insensitive to coupling constants in our theory, originates from the cancellation of the same RG renormalized running coupling constant $g^2(\ell)$ in Σ_ξ and in the denominator of $\mathcal{G}_\xi$ (arising from the second-order hopping process that generates dynamics and energy dispersion of the ξ-band). Due to this cancellation, all initial (bare) values of $\bar{g}$ and J which flow to the U(1) FL* fixed point at $\bar{g} = J = 0$ form an extended 'phase' by showing the same Planckian strange-metal behavior (see equation (8)).

Note that equation (8) is a generic universal (coupling-constant independent) scattering rate we predict for the universal Planckian metal states observed in cuprates. However, there is a broad implication of our equation (8) for other materials: it appears that this coupling-constant independent universal scaling form might not be unique to cuprates, and

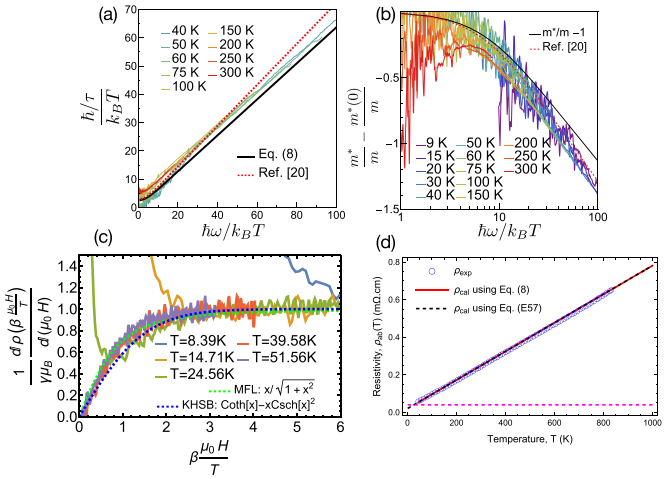

Figure 4. ω/T scaling of scattering rate and the effective mass enhancement. Theoretical fitting for both (a) the scattering rate $\hbar/\tau$ and (b) the effective mass enhancement $m^*/m-1=g(x)$ from our theory exhibits a universal scaling behavior as a function of $x\equiv\hbar\omega/k_BT$ (black solid lines). The function $g(x)$ is defined in equation (F13) of appendix F2. In addition, theoretical results of $\hbar/\tau$ and $m^*/m-1$ obtained in [20] are added for comparison (red dashed line). The experimental data shown in (a) and (b) is reproduced from [20]. (c) Derivative of the magnetoresistance, divided by $\gamma\mu_B$, for Tl2201 with $T_c=23$ K at various temperatures collapses onto a universal scaling function given by equation (9) when X is replaced by $\frac{\beta\mu_0 H}{T}$. Here, $\beta\simeq 4.66$ and $\gamma\mu_B\simeq 0.0049$ are fitting parameters. Additionally, the scaling behavior of the magnetoresistance derivative can also be described by an alternative Marginal Fermi-Liquid (MFL) form (green dashed line) given in equation (F9). For further details, see appendix F1. Magnetoresistance at $T_c=26.5$ K exhibits similar scaling, as shown in figure S4 in appendix F1. Experimental data in (c) is reproduced from [21]. (d) Resistivity calculated from the scattering rate predicted within our theory (equation (8)) (red line) and equation (E57) (black dashed line) using the DC Drude formula $\rho_{ab}=(m^*d/ne^2)(1/\tau)=A_1T$ where $d=0.64$ nm [72] is the interlayer spacing and where $A_1=(8/\pi)(k_B/\hbar)((m^*d)/(ne^2))$, obtained by taking the DC limit of equation (8), m^*/ne^2 with $n=(1-\delta)/(a^2)=5.95\ (\mathrm{nm})^2$, $a=0.378$ nm, [72] $\delta=0.15$, $m^*=5.8m_b$ (red line) and $m^*=16.69m_b$ (black dashed line), m_b being the bare electron mass, which agrees with estimation from [2] and with the high-T static value of the effective mass in [20] (red line), with for comparison in-plane resistivity data (blue circles) reproduced from [19] showing T-linear dependence up to 800K. From equation (E57), we also fitted the observed residual resistivity $\rho_0\approx 0.02\mathrm{m}\Omega\cdot$ cm by the constant $\rho_0=m^*\mathrm{d}A/(ne^2\hbar)$ where we find that $A\approx 2\cdot 10^{-3}$eV. Equation (E57) is valid below the horizontal pink dashed line.

could in general describe systems other than cuprates. This further suggests that the cancellation in coupling constant dependence in the electron self-energy (or scattering rate) is likely a generic feature of universal Planckian metal state and expected to also occur in other materials showing similar universal Planckian metal behavior. Nevertheless, the constant pre-factor $4/\pi$ in equation (8) is unique to our specific t–J model for cuprates, and this value may vary within different models. Whether our result also applies to other materials showing similar Planckian metal behavior deserves further study.

Since the whole T-linear mystery and its phenomenological description via the MFL theory lays in the T-linear behavior extending from very low up to high temperatures, we further extract the DC-resistivity from the most general form of equation (8), valid for any finite temperatures in the scaling regime. By taking the DC-limit ($\omega\to 0$) in equation (8), a perfect T-linear resistivity, ranging from very low to very high temperatures, can be derived via the Drude formula: $\rho=(m^*/ne^2)(1/\tau)=A_1T$ where $A_1=(8/\pi)(k_B/\hbar)(m^*/ne^2)$. Note that in 2D metallic systems with isotropic Fermi surface, close to our case for SM phase, n/m^* can be considered as a temperature-independent constant fixed by the Fermi energy ϵ_F via $\epsilon_F=\hbar^2{k_F}^2/2m^*$ with $n\propto {k_F}^2$. By a reasonable estimate of n/m^* value, the T-linear resistivity data for LSCO in reference [19] is well fitted by our theory for DC-resistivity based on equation (8) (see figure 4(d)). The quantum critical scenario we propose here offers a mechanism for explaining the T-linear mystery– T-linear resistivity observed (in Tl-2201 or LSCO) extending from 7–38 K up to 700–1000 K without changes in slope and having T as the only visible scale–since temperature is the only relevant scale in the quantum critical region. In appendix E4, we derive the similar T-linear resistivity via an alternative approach by a low-temperature expansion within the Boltzmann transport formula, see equation (E57), which also provides a good fit to the experimental data for T linear resistivity (see figure 4(d)).

Meanwhile, the electron mass renormalization $m_e^*-m_e^*(0)$ is well captured by a universal scaling form: $m_e^*/m_e(0)-1=g(x)$ with the scaling function $g(x)$ obtaining from the real part of the dynamical self-energy Σ'_ξ via Kronig–Kramers relation (see figure 4(b) and appendix G).

Moreover, we find that the magnetoresistance derivative $\mathrm{d}\rho(H,T)/\mathrm{d}\mu_0H$ in the strange-metal region of cuprate superconductor at finite temperatures and external magnetic fields (but zero frequency) observed in [21] is well-described by the universal quantum critical scaling in the frequency-derivative of AC-resistivity $\mathrm{d}\rho(\omega,T)/\mathrm{d}\hbar\omega$, predicted within our theory for the entire Planckian metal phase (assuming $\hbar\omega$ plays an effective role as magnetic field μ_0H in the scaling region). As shown in figure 4(c), across the extended strange-metal region, the field derivative of magnetoresistance of

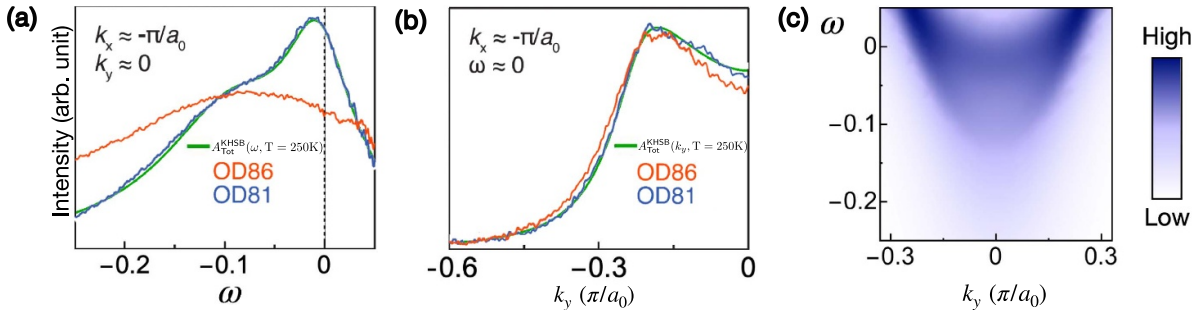

Figure 5. Spectral intensity for the SM phase: (a) Spectral weight as a function of frequency ω at the anti-nodal point, and (b) spectral weight as a function of momentum k_y at a zero frequency. Experimental data OD86 (red) and OD81 (blue) are reproduced from [40]. Greens curves in (a) and (b) corresponds to our theoretical fitting to OD81, with temperature being fixed at $T = 250$ K. (c) Density plot for the spectral weight as a function of ω and k_y (see appendix G for details).

overdoped cuprates exhibits a doping-independent, universal H/T scaling: $(\gamma\mu_{\rm B})^{-1}{\rm d}\rho(H,T)/{\rm d}(\mu_0 H) = \beta X/\sqrt{1+(\beta X)^2}$, where α and γ are fitting parameters, and $\beta \equiv \gamma\mu_{\rm B}/\alpha k_{\rm B}$ and $X \equiv \mu_0 H/T$ here. By the following identifications, $\alpha \to 8m^\star/\pi ne^2$, $\gamma\mu_{\rm B} \to 2m^\star/\pi ne^2$, $\mu_0 H \to \hbar\omega/4$, we find that the frequency derivative of the AC resistivity $\rho(\omega,T) = (m^\star/ne^2)(1/\tau(\omega,T))$ from our theory agrees well with the experimental results for $(\gamma\mu_{\rm B})^{-1}{\rm d}\rho(H,T)/{\rm d}(\mu_0 H)$ (see the blue dashed line of figure 4(c)):

$$\frac{ne^2}{m^\star} \times \frac{\pi}{2}\frac{{\rm d}\rho(\omega,T)}{{\rm d}(\hbar\omega)} = \coth(X) - X{\rm csch}^2(X), \qquad (9)$$

with $X = \hbar\omega/4k_{\rm B}T$ in equation (9). This suggests that frequency and magnetic field play equivalent roles near quantum criticality associated with the SM state. Note that the interpretation of B/T-scaling in cuprates is still controversial. A a different interpretation of the B/T-scaling in some cases based on ordinary electrons has been reported in [75].

2.3.3. Single-particle spectral function. Our theory offers a mechanism for the phenomenological MFL ansatz [66]: The complete electron self-energy Σ_ξ, is reminiscent of the MFL behavior with a distinction that Σ_ξ here is insensitive to coupling constant. The resulting single-particle spectral function $A(\omega,\boldsymbol{k},T) \equiv -\pi^{-1}G_c^R(\omega,\boldsymbol{k},T) = -\pi^{-1}{\rm Re}\left[\omega - \varepsilon_{\boldsymbol{k}} - \Sigma_c\right]^{-1}$ thus shows an excellent fit to the recent ARPES measurement for overdoped cuprates in the SM region [40] (see figure 5 and appendix G).

2.3.4. SM state: signature of QCP vs. quantum critical phase. Our RG results offer further insights to the issue on the origin of the Planckian SM state. The RG flow in figure 3(a) in general may lead to three distinct temperature-doping (T,δ) phase diagrams by following the three paths I, II, and III depending on initial values of t and J with increasing doping, see figures 3(b)-I, (b)-II, (b)-III. Experimentally, the three paths can be tuned by magnetic fields: When the external magnetic field is weak, the couplings lie on path I in which a finite range of couplings on this path flow to the superconducting phase. This corresponds to figure 3(b)-I. At a critical magnetic field, couplings follow path II and pass through the QCP at C_r; consequently, the SM state at finite T is controlled by a single QCP. The most interesting case, however, is path III, occurring at a larger field which completely suppresses superconductivity. For path III, there is a finite range of doping where all initial values of t and J (blue solid line in path III of figure 3(a)) flow to the SM fixed point. In this case, the Planckian SM behaviors at finite T persist over a finite doping range as $T \to 0$, corresponding to the quantum critical SM 'phase'. Experimental signatures of both QCP [34, 41] and quantum critical phase [21] were reported in different cuprates. These seemingly incoherent results can be coherently unified in our generic RG phase diagram: the former may follow a path close to path II, while the latter follows path III.

2.3.5. Thermodynamic property: divergence of specific heat coefficient at the QCP. We further computed the specific heat coefficient in the SM phase near the QCP, which shows logarithmic-in-T MFL behavior: $C_V/T \sim -[A + B(J)]\ln T$ with A being a constant and $B(J)$ is a power-law divergent prefactor arising from quantum critical antiferromagnetic short-ranged spin fluctuations (the J term): $B(J) \sim |J - J_c|^{-p}$ with $p = \nu/2 = 1/2$, see appendix D for the estimation of $B(J)$. This power-law behavior of C_V/T aligns well with the experimentally observed power-law divergence specific heat coefficient at low temperatures in Eu-LSCO and Nd-LSCO near the pseudogap critical point [34, 41], i.e. $C_V/T|_{T\to 0} \sim |\delta - \delta_c|^{-m}$ with $m \sim 0.5$, as shown in figure 6. The dominant logarithmic-in-T dependence, $-B(J)\ln T$, in our theory originates from the van Hove singularity (VHS) of the half-filled f-spinon band on a 2D square lattice (see the spinon Fermi surface in figure 1(b) and appendix D), while the subleading constant term $-A\ln T$ is contributed from the self-energy $\Sigma_{c,f}$.

It was pointed out in [41] that the VHS in the electron DOS could not simply account for the $\log(1/T)$ divergence of the specific heat because of disorder and/or interplane hopping. Nevertheless, we think that VHS of f spinons is more robust against disorder and/or interplane hopping compared to that from the electron band. The reasons are as follows. Firstly, the occupation for f–spinons in SM phase where slave bosons are non-condensed ($\langle b_i\rangle = 0$) is fixed to half-filling with VHS Fermi surface ($f_{i\sigma}^\dagger f_{i\sigma} = 1$) by the local slave-boson constraint:

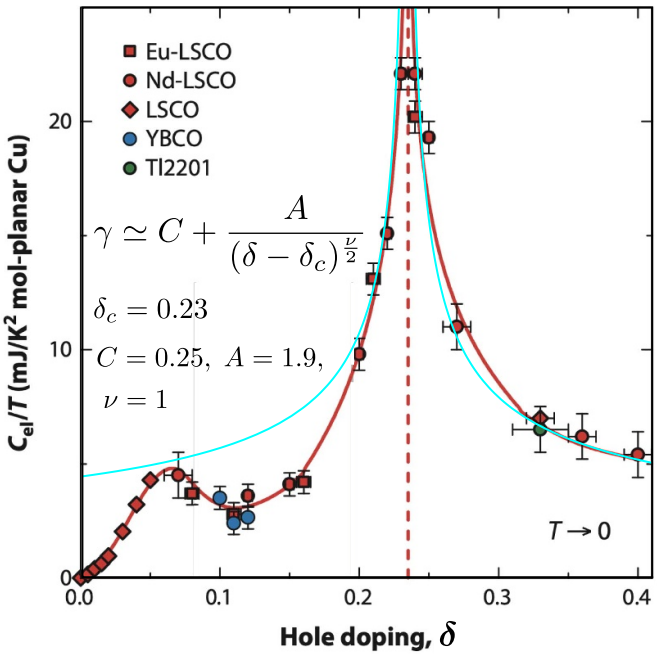

Figure 6. Power-law divergence of the electronic specific heat coefficient C_V/T for various samples around the optimal doping. Experimental data are reproduced from [41]. The blue line corresponds to the power-law fit (cf equation (D8)).

$f^\dagger_{i\sigma} f_{i\sigma} + b^\dagger_i b_i = 1$. In our SM phase extended to a finite doping range (with a small Fermi surface), the f spinons always stay at half-filled as doping is varied over the entire phase. This makes f spinon Fermi surface robust against doping. Secondly, the 2D charge-neutral f spinons are stabilized by forming RVB singlets, and are expected to be less affected by the charged disorder and/or interplane charge transfer. Nevertheless, the spinon Fermi surface should change when the electron Fermi surface changes from small to large. This should shift the spinon Fermi surface away from the VHS. When this occurs, the system already reaches the FL phase, and the VHS effect is suppressed. The T-logarithmic singular specific heat coefficient is expected to be smeared out (see figure 7(a) in [34]).

2.3.6. Fermi surface reconstruction across the SM region. Our heavy-fermion two-band formulation of the slave-boson t–J model offers a natural explanation on the enlargement of FS)volume from a smaller FS with hole density δ in pseudogap phase to a larger one with hole density $1+\delta$ in the FL phase ($\langle b\rangle = \sqrt{\delta},\ \xi_\sigma \sim \sqrt{\delta} f_\sigma,\ \sum_\sigma f^\dagger_{i\sigma} f_{i\sigma} = 1-\delta$) across the SM region (figure 1(b)) [21, 76, 77].

In the pseudogap and SM phases with non-condensed bosons, the ξ-band shows a small hole Fermi surface (hole doping δ). When bosons get condensed across the FL phase boundary, the Fermi surface volume undergoes a sudden jump from δ to $1+\delta$, in parallel to that occurred at Kondo-breakdown transition in heavy-fermion systems [35, 36]. This is due to the participation of the half-filled spinon band to the Fermi surface by Kondo hybridization between the f- and the ξ-bands; therefore the hole Fermi surface volume of a normal conduction electron band with a hole density $1+\delta$ (corresponding to a doped hole density δ relative to half-filling) is recovered, in accordance with the Luttinger theorem (see figure 1(b)). This scenario offers a qualitative understanding of the rapid increase observed in the normal-state Hall number near the critical doping of YBCO and Nd-LSCO [34].

Nevertheless, a smooth crossover of the Fermi surface volume from δ to $1+\delta$ is possible in the SM phase via a mixture of two fluids: (i) normal metal with T-quadratic resistivity by partial boson condensation and a large Fermi surface volume ($1+\delta$), and (ii) SM with T-linear resistivity without boson condensation and with a small Fermi surface volume (δ). This two-fluid picture may arise within our model when the mean-field slave-boson b-field get partial condensation, $\langle b\rangle = x < \sqrt{\delta}$. As one goes from SM to FL phases, the condensate fraction is expected to increase with increasing doping till a full condensation $x = \sqrt{\delta}$ is reached. The partially condensed slave-boson in principle exists as a possible solution of our mean-field equations. When this occurs, two types of conduction electrons—the normal electrons and the SM electrons—may co-exist. The normal electron band shows a large Fermi surface and T-quadratic resistivity linked to condensed bosons, while the SM electron band exhibits a small Fermi surface and T-linear resistivity linked to the non-condensed bosons. Both kinds of electrons are coupled through Kondo-like effective hopping term of our model and are expected to contribute to the total Fermi surface. Therefore, a smooth crossover of the Fermi surface volume from δ to $1+\delta$ is possible in the SM phase by a mixture of the small and large Fermi surfaces. This two-fluid picture resembles the mixture of T-linear and T-quadratic resistivity in SM region of certain cuprates where a smooth change in Fermi surface volume from Hall coefficient measurement was observed [21]. Further study on our proposed scenario is needed.

3. Discussions

First, we make some remarks on the rich phenomena of the pseudogap phase in cuprates, possible theoretical proposals for its origin, as well as experimental evidence for the RVB preformed Cooper pair in this phase, supporting our theoretical framework for the pseudogap phase. The pseudogap phase shares the phase boundary with SM state by T^* line (onset temperature of a spin-gap) on the underdoped side. It is a much poorly conducting phase (compared to the SM and the FL phases) where resistivity increases with decreasing temperatures due to the suppression of electron local density of states near the Fermi energy by developing the spin gap near anti-nodal points. The T^*-line approximately marks the different transport behaviors between the pseudogap and the SM phases. As a result, with decreasing temperature across T^* line from above, the system changes from the SM state with T-linear decreasing resistivity to the pseudogap state with resistivity increased with decreasing T.

The origin of the pseudogap phase of cuprates is a long-standing debated issue. There have been different opinions

regarding this enigmatic phenomena. These different opinions in the literature can be approximately classified into two different groups with qualitatively two different kinds of origins proposed for the pseudogap phase [78, 79]: 1. it is caused by the preformed Cooper pairing for $T > T_c$, following the idea of Anderson's RVB singlet pairing; 2. it is due to some broken symmetry phases, such as: pair-density-wave state [80], time-reversal symmetry broken (loop-current state) [67], or the nematic phase [56]. However, it goes beyond the scope of our paper to discuss and compare these different proposals in great details. Here, we follow the first proposal above by assuming the pseudogap phase is mainly driven by the RVB singlet preformed Cooper pairs.

There are a number of experimental evidences to support the existence of Cooper pairing in the pseudogap phase. As pointed out in [81], superconducting (Bogoliubov) quasiparticle peaks observed in ARPES, a signature of strong superconducting fluctuations, have been observed in the pseudogap region of cuprates for $T_c < T < T_{\rm pair}$ with $T_{\rm pair} < T^*$ (immediate above the superconducting dome or in between T^* line and the superconducting phase). This behavior has been interpreted as a signature of preformed Cooper pairing and was considered as one prominent candidate to explain the pseudogap: the strong superconducting fluctuations above T_c destroy phase coherence but not the pairing [82]. Nevertheless, the Cooper-pair formation above T_c is somewhat disentangled from the pseudogap state or $T_{\rm pair}$ does not fully coincide with T^*. Similar behavior has been observed in [78, 83]. A recent experimental evidence in [79] was reported to more directly and strongly tie pseudogap state to the formation of preformed Cooper pairing in cuprates by low temperature local shot-noise spectroscope. The shot-noise power S_I is proportional to the quasi-particle charge q, $S_I = 2q|I|$ with I being the tunneling current. For normal state electron tunneling, $q = e$, while as $q = 2e$ for Cooper pair tunneling. Their data from differential conductance spectra shows that the pseudogap energy $\Delta_{\rm PG}$ (the size of pseudogap with suppressed tunneling density of states) coincides with the onset energy scale of Cooper pairing $\Delta_{\rm pair}$ where quasi-particle charge shows a sharp increase from $q = e$ to $q > e$ with decreasing energy. The authors interpret their results as a demonstration of equivalence of pseudogap and pairing energy. Though the origin of the pseudogap is still a much debated open problem, we think our proposal—pseudogap state as a preformed Cooper pairing state—is justified to be a reasonable scenario supported by various experiments, and it serves as an appropriate starting point to address the quantum critical SM phase in cuprates.

We now comment on the possible occurrence of broken symmetry phases (such as: dimerization, flux phase formation) within our mean-field theory. Although it is quite likely that these broken symmetry states are not occurring at the sizable doping relevant for the SM QCP, it is worthwhile discussing to what extent the uniform RVB state is stable. It is known that within mean-field approaches to Hubbard and t–J model close to the half-filling on square lattice with only nearest-neighbor couplings the uniform RVB state is unstable against formation of broken symmetry phases, such as: dimerized or flux phases. For example, in the large-N [SU(N)] approach to the half-filled Hubbard-Heisenberg model studied in [84], in the square lattice limit and with decreasing J/t ratio, the uniform RVB state is first unstable against the dimerized plaquette (box) phase at large J/t, then is unstable against the flux phase for smaller J/t till $J/t \to 0$. For a realistic value of $J/t \sim 0.3$ in the t–J model close to half-filling, the flux phase is expected to be the ground state. The authors in [32] discussed this issue and found that replacing uniform RVB by the staggered flux phase will not change the electronic observables. This is because the ξ-fermions, carrying the gauge charge of 2, pick up an Aharonov–Bohm phase of 2π when circulating an elementary plaquette, which leaves their low energy properties unchanged. Nevertheless, the uniform RVB phase can be stabilized by introducing a small next-nearest-neighbor hopping t' and Heisenberg exchange J' terms as studied in [84].

It is known that in the absence of SC the spin-liquid Kondo lattice investigated in [33] is unstable towards phase separation (see, e.g. [85]). To address this issue, we solved the mean-field saddle-point equations of our KHSB t–J model. We find the compressibility of the fermion fields in the SM, pseudogap, and SC phases are all positive and finite, indicating that the mean-field phases of our model are stable against phase separation (see appendix H for details). A possible reason to explain the phase separation tendency in [85] would be as follows: The strong Kondo hybridization therein is dispersive (momentum dependent). In terms of slave-boson representation of the Kondo hybridization, it implies the slave-bosons are very mobile. As a result, they tend to group together spatially, separated from the spinons, to gain kinetic energy by hopping between them. Thus, the total free energy is further reduced. By contrast, our slave bosons (Kondo hybridization) are local, dispersionless with much weaker in strength ($\langle b \rangle \sim x < \sqrt{\delta}$). Therefore, the phase separation does not occur here.

In [32] section V.B, the authors emphasizes the difficulties for their model in describing the transition from the U(1)-FL* phase to the FL state. In particular they mention that a continuum theory with a finite Fermi velocity for the composite fermionic fields F (the ξ-fields here) would not be compatible with the hard-core dimer constraint which the F field must obey at the lattice level. We think the origin of this difficulty lies in the fact that the effective action for the F-fermions (equation (29)) is obtained from the effective action (equation (11) therein) where both slave-bosons and f-spinons have already been integrated out. As a result, the F-fermions in equation (11) does not lead to a quadratic dispersion on square lattice due to the hard-core dimer constraint. By contrast, both f-spinon and slave-boson fields in our effective action (our equation (1)) are kept intact (without being integrated out). We find that the dynamics and quadratic band dispersion of our ξ-fermions can be generated perturbatively by calculating the leading non-trivial self-energy correction, Σ_ξ, via Random Phase Approximation approach where the dynamics and dispersion of the ξ fermion are generated by integrating out the higher energy modes in its self-energy. (see appendix B for details). Therefore, the above difficulty does not appear within our effective action, and the U(1)-FL*-FL phase transition can be captured here.

The Umklapp scattering is usually expected to be important for electrical resistivity by relaxing electron momentum (charge current). Here, we propose an alternative relaxation mechanism without Umklapp scattering via local charge Kondo fluctuations where electrical charge current decays into charge-neutral spinon current and local charge fluctuations despite forward scattering [86].

Note that the $U(1)$ gauge field fluctuations play an important role in the traditional $U(1)$ slave boson approach to t–J model [28, 29]. Within this approach, the quasi-particle mass and dispersion are generated by the single electron Green's function, a convolution of spinon and holon (slave-boson) Green's function, where the massive gauge field fluctuations play an important role to get the finite quasi-particle mass $m^* \sim 1/J$ in the half-filled limit ($\delta \to 0$). Similarly, the gauge field fluctuations lead to ac-conductivity $\sigma_{ac}(w) \sim \delta/m\delta(w)$, which vanishes in the Mott limit ($\delta \to 0$). We find that the contributions from gauge field fluctuations are also present in our approach to the slave-boson t–J model. However, due to the much heavier ξ-band compared to that of f-spinon, we find that their contributions are subleading and are negligible compared to the leading Planckian scattering rate mentioned above, within the temperature range of our interest (see appendix E): $\left(1/\tau_{\xi}^{\text{gauge}}\right)/(1/\tau_{\xi}) \sim (T/D)^{1/3}(t/D)^2\delta^2 \ll 1$. Similarly, the scattering rate contributed from the gauge field coupled to the spinon is estimated as: $\left(1/\tau_{f}^{\text{gauge}}\right)/(1/\tau_{\xi}) \sim (T/D)^{1/3} \ll 1$. By including the gauge filed fluctuations, we find that the total resistivity ρ_{tot} is approximately given by $\rho_{\text{tot}} \sim \rho_{\xi}$, as $\rho_{\xi}^{\text{gauge}}/\rho_{\xi} \ll 1$ and $\rho_{f}^{\text{gauge}}/\rho_{\xi} \ll 1$. The total ac-conductivity is approximated given by the conductivity of the ξ-field: $\sigma_{\text{tot}}(\omega) = 1/\rho_{\text{tot}}(\omega) \sim \sigma_{\xi}(\omega)$. We find that $\sigma_{\xi}(\omega)$ within our approach does indeed recover the expected Mott physics in $\delta \to 0$ limit: $\sigma_{\xi}^{\text{AC}}(\omega) \sim \delta \times \delta(\omega)$ [87]. We also find that gauge field leads to a negligible contribution to our specific heat coefficient: $\gamma(T) \sim (b/D) \times (T/D)^{2/3}$ with $b \sim O(\delta^2) \ll 1$. Meanwhile, due to the much narrow ξ-band (or heavy effective mass of the ξ-field), the physical quasi-particle mass is dominated by m_{ξ} though there exists a negligible contribution from the single-electron Green's function convoluted by spinon and holon Green's function via [28] where gauge field plays an important role. We find that the quasi-particle mass of the ξ-field behaves as: $m_{\xi} \propto 1/(\delta J)$, which diverges in $\delta \to 0$, recovering the Mott insulating phase of the half-filled Hubbard model with divergent quasi-particle mass $m^* \sim 1/\delta$, as was proposed by Anderson [88]. Very recently, there has been new experimental evidence for this Mott physics relation with $m^* \sim 1/\delta$ to exist for a wide doing range ($0.1 < \delta < 0.3$) in cuprate (LSCO) [3] by measuring the slope (A_1 coefficient) of T-linear resistivity $\rho \sim A_1 T$ with $A_1 \propto m^* \propto 1/\delta$ and specific heat coefficient $\gamma \propto m^* \propto 1/\delta$. Note that, due to the local nature of the slave boson in our approach, the T-linear scattering rate contributed from U(1) gauge field found in [28] is absent here.

We summarize the main difference between our heavy-fermion approach and the traditional approach [28] to the slave-boson t–J model in describing the SM state as follows: The key difference is the different mean-field decoupling of the slave-boson hopping term $H_t = -t\sum_{\langle i,j\rangle,\sigma} f_{i\sigma}^{\dagger} b_i b_j^{\dagger} f_{j\sigma} + \text{H.c.}$. In traditional mean-field approach, $H_t \to \sum_{\langle i,j\rangle}\left(-t\chi_{ij} b_i^{\dagger} b_j + \text{H.c.} + |\chi_{ij}|^2/t\right)$, while as in our approach $H_t \to \sum_{\langle i,j\rangle,\sigma}\left(-t f_{i\sigma}^{\dagger}\xi_{ij,\sigma} b_j^{\dagger} + \text{H.c.} + |\xi_{ij,\sigma}|^2/t\right)$. Within our approach, by defining the charge-carrying fermionic spinon-holon bound pair (ξ-field), the physical conduction (hole) band comes directly from the hopping of the ξ-field via second-order in perturbation at the Hamiltonian level. The slave-bosons are treated as local non-condensed disordered charge impurity. This formulation facilitates to qualitatively describe the observed Fermi-arc near nodal points in the pseudogap phase [32], the strange metal ground state (phase) and the Fermi surface reconstruction across it, as well as the phase transitions between the SM phase and its neighboring phases (pseudogap, d-wave superconducting, and FL phases). The heavy ξ-band strongly suppresses the gauge field contributions to observables. By contrast, within the traditional U(1) slave-boson approach to t–J model, both sipnons and holons (slave-bosons) are mobile and acquire bands. The physical electron (hole) band is formed indirectly through convolution of spinon and holon Green's functions where gauge field plays an important role. Meanwhile, since slave-bosons are mobile within this approach, they always get Bose-condensed for $T < T_{\text{BEC}}$ with T_{BEC} being the Bose–Einstein condensation temperature. As a result, the ground state is a superconducting state for any finite doping before the system reaches the FL phase. Hence, the SM state always remains in the normal state and is unstable against superconductivity as $T \to T_{\text{BEC}}$ from above.

The Planckian metal phase we find here can be further stabilized in the generalized version of our model in large-N and multi-channel limit where fluctuations from gauge-field and higher order processes are suppressed. The Planckian phase in transport and thermodynamical coefficients within our theoretical framework show distinct qualitative features: the former is insensitive to but the latter strongly depend on the microscopic couplings. This suggests possible breakup of low-energy excitations in this phase into charged particles (electrons) and the charge-neutral spinons; the former dominates in transport while the latter in thermodynamics, reminiscent of the Kondo breakdown QCP in heavy-fermion system [12]. In addition, Whether the quadratic temperature dependence of the Hall angle observed in the SM region of cuprates [16, 89–91], can be captured within our framework requires further investigation .

To reach the Planckian bound, it was argued in [18] that a strong inelastic scattering with local energy relaxation $\Delta E \sim k_{\text{B}}T$ is required so that the equilibration time $\tau_{\text{eq}} \sim \hbar/\Delta E \sim \hbar/k_{\text{B}}T$ reaches the Planckian time scale. The charge fluctuating effective Kondo term in our model offers a realization of such strong inelastic scattering channel with a local energy relaxation rate $1/\tau \sim k_{\text{B}}T/\hbar$, where electron loses its energy to local slave boson by coupling to a spinon band.

It was pointed out that the strong disorder coupled to the electron interactions is crucial to realize the Planckian SM

state, as shown in the SKY model [24, 25]. Within our two-band heavy-fermion slave-boson t–J model, local fluctuating non-condensed slave boson plays the role of disorder embedded in electron interaction in the fluctuating Kondo hybridization. MFL and SM properties are thus expected, reminiscent of the SKY models. Via the effective Kondo term, the fluctuating slave-boson also generates impurity-like scattering, leading to a residual scattering rate at $T = 0$ due to the breaking of the translational symmetry of the original Hamiltonian. A formal link of our model to the SYK-like models deserves further investigations.

Note that there exists materials (such as: $Nd_xCe_{1-x}CoIn_5$ in [17]) which show T-linear scattering rate with a non-universal (coupling-constant dependent) Planckian coefficient ($\alpha \sim 1$ but α depends on microscopic coupling constants). The mechanism for these materials is expected to be different from those with universal Planckian coefficient since the cancellation in coupling constant dependence in scattering rate is absent there.

Our mechanism shows a broader implication for the SM state observed in other correlated unconventional superconductors, such as: in Magic-Angle Twisted Bi-layer Graphene (MATBG) [14, 92] where the universal scaling in Planckian scattering rate was observed, and in nickelate superconductors [93] where a T-linear resistivity was observed in the quantum-critical-fan-like region above the superconducting phase, similar to that in cuprates. A topological heavy-fermion Anderson/Kondo lattice approach to MATBG was proposed to account for its flat-band structure [94–97]. We expect the possible enhanced charge fluctuations via Kondo hybridization in the spin sector above the superconducting transition temperature of MATBG, similar to that for our case in the charge sector, may play a role to account for the observed Planckian scattering rate. Meanwhile, the Kondo–Hubbard model was proposed to serve as a promising minimum microscopic model for the newly discovered nickelate superconductors [98], where the local Kondo-breakdown transition, similar to our case, may occur. The combined quantum critical bosonic charge fluctuations in the correlated electron hopping and Kondo interaction in the putative quantum critical region may provide a mechanism for its SM behavior. Our theoretical study on Planckian metal in cuprates sheds lights on the understanding of the Planckian metal states in other materials since 1. cancellation in coupling constant dependence (or coupling-constant free) in scattering rate is likely a generic feature of universal Planckian metals across different materials, and 2. we offer one mechanism for such cancellation in a model for cuprates. Further extension of our approach is needed to clarify these issues.

4. Conclusions

We provide a microscopic mechanism for the Planckian metal phase in the Kondo–Heisenberg formulation of the slave-boson t–J model based on the dynamical charge Kondo breakdown near the localized-to-delocalized phase transition in the form of critical charge (Kondo) fluctuations. The slave-boson t–J model was first mapped onto an effective Kondo–Heisenberg model. Via perturbative RG analysis on this effective model, we realized an extended quantum critical Planckian metal phase. Within the one-loop RG, we identified a QCP separating pseudogap, d-wave superconducting, a normal FL and a SM phases. In particular, we find a stable SM phase in our RG phase diagram close to this critical point exhibiting T-linear scattering rate and ω/T-quantum critical scaling and the Planckian behavior where $\alpha_P \sim O(1)$ that is independent of coupling constant, in excellent agreement with the optical conductivity and magnetoresistance measurements in various overdoped cuprates. Our theoretical predictions on the specific heat coefficient, effective mass enhancement, and single particle spectral function in the SM state agree well with the experimental observations and hence offers a microscopic mechanism for the marginal FL Ansatz. Our theoretical framework offer a promising route to reveal the mystery of quantum critical SM phase and its link to the generic phase diagram of high-T_c cuprate superconductors. It provides insights into how dSC emerges from such a SM phase in cuprates–one of the long-standing open problems in condensed matter physics since 1990s–as well as shows a broader implication for Planckian SM states observed in other correlated unconventional superconductors.

Data availability statement

All data supporting the findings of this study are available upon reasonable request. The data that support the findings of this study are openly available at the following URL/DOI: https://doi.org/10.5281/zenodo.14848163.

Acknowledgment

We acknowledge discussions with Cenke Xu, G Kotliar, A Georges, J Schmalian, E Berg, T Devereaux, S A Kivelson, P A Lee, T K Lee, P Coleman, N Hussey, R Greene, B Michon, D Van Der Marel. We also acknowledge Dr Po-Hao Chou for discussions and technical support. This work is supported by the National Science and Technology Council (NSTC) Grants 110-2112-M-A49-018-MY3, the National Center for Theoretical Sciences of Taiwan, Republic of China (C- H C). Y-Y C acknowledges the financial support from The 2023 Postdoctoral Scholar Program of Academia Sinica, Taiwan. C-H C acknowledges the hospitality of Aspen Center for Physics, USA and Kavli Institute for Theoretical Physics, UCSB, USA where part of the work was done. This research was supported in part by grant NSF PHY-2309135 to the Kavli Institute for Theoretical Physics (KITP).

ORCID iDs

Yung-Yeh Chang https://orcid.org/0009-0008-3537-5984
Khoe Van Nguyen https://orcid.org/0000-0002-7966-2669
Kim Remund https://orcid.org/0000-0003-2445-6777
Chung-Hou Chung https://orcid.org/0000-0002-1502-6022

References

[1] Fournier P, Mohanty P, Maiser E, Darzens S, Venkatesan T, Lobb C J, Czjzek G, Webb R A and Greene R L 1998 *Phys. Rev. Lett.* **81** 4720
[2] Legros A *et al* 2019 *Nat. Phys.* **15** 142
[3] Shekhter A, Ramshaw B J, Chan M K and Harrison N 2024 Mott physics and universal Planckian relaxation in the high-T_c cuprates (arXiv:2406.12133 [cond-mat.str-el])
[4] Hussey N E, Buhot J and Licciardello S 2018 *Rep. Prog. Phys.* **81** 052501
[5] Licciardello S, Buhot J, Lu J, Ayres J, Kasahara S, Matsuda Y, Shibauchi T and Hussey N E 2019 *Nature* **567** 213
[6] Kasahara S *et al* 2010 *Phys. Rev.* B **81** 184519
[7] Jiang S, Xing H, Xuan G, Wang C, Ren Z, Feng C, Dai J, Xu Z and Cao G 2009 *J. Phys.: Condens. Matter* **21** 382203
[8] Huang W K *et al* 2020 *Phys. Rev. Res.* **2** 033367
[9] Doiron-Leyraud N, de Cotret S R, Sedeki A, Bourbonnais C, Taillefer L, Auban-Senzier P, Jérome D and Bechgaard K 2010 *Eur. Phys. J.* B **78** 23
[10] Bruin J A N, Sakai H, Perry R S and Mackenzie A P 2013 *Science* **339** 804
[11] Gegenwart P, Custers J, Geibel C, Neumaier K, Tayama T, Tenya K, Trovarelli O and Steglich F 2002 *Phys. Rev. Lett.* **89** 056402
[12] Custers J, Gegenwart P, Wilhelm H, Neumaier K, Tokiwa Y, Trovarelli O, Geibel C, Steglich F, Pépin C and Coleman P 2003 *Nature* **424** 524
[13] Custers J, Gegenwart P, Geibel C, Steglich F, Coleman P and Paschen S 2010 *Phys. Rev. Lett.* **104** 186402
[14] Cao Y, Chowdhury D, Rodan-Legrain D, Rubies-Bigorda O, Watanabe K, Taniguchi T, Senthil T and Jarillo-Herrero P 2020 *Phys. Rev. Lett.* **124** 076801
[15] Zaanen J 2004 *Nature* **430** 512
[16] Phillips P W, Hussey N E and Abbamonte P 2022 *Science* **377** 169
[17] Chang Y-Y, Lei H, Petrovic C and Chung C-H 2023 *Nat. Commun.* **14** 581
[18] Hartnoll S A and MacKenzie A P 2022 *Rev. Mod. Phys.* **94** 41002
[19] Takagi H, Batlogg B, Kao H L, Kwo J, Cava R J, Krajewski J J and Peck W F 1992 *Phys. Rev. Lett.* **69** 2975
[20] Michon B, Berthod C, Rischau C W, Ataei A, Chen L, Komiya S, Ono S, Taillefer L, van der Marel D and Georges A 2023 *Nat. Commun.* **14** 3033
[21] Ayres J *et al* 2021 *Nature* **595** 661
[22] Sarkar T, Mandal P R, Poniatowski N R, Chan M K and Greene R L 2019 *Sci. Adv.* **5** eaav6753
[23] Jin K, Butch N P, Kirshenbaum K, Paglione J and Greene R L 2011 *Nature* **476** 73
[24] Patel A A and Sachdev S 2019 *Phys. Rev. Lett.* **123** 066601
[25] Patel A A, Guo H, Esterlis I and Sachdev S 2023 *Science* **381** 790
[26] Patel A A, Lunts P and Sachdev S 2024 *Proc. Natl Acad. Sci.* **121** e2402052121
[27] Huang E W, Sheppard R, Moritz B and Devereaux T P 2019 *Science* **366** 987
[28] Nagaosa N and Lee P A 1990 *Phys. Rev. Lett.* **64** 2450
[29] Lee P A and Nagaosa N 1992 *Phys. Rev.* B **46** 5621
[30] Lee P A, Nagaosa N and Wen X-G 2006 *Rev. Mod. Phys.* **78** 17
[31] Varma C M 2016 *Rep. Prog. Phys.* **79** 082501
[32] Brunkert J and Punk M 2020 *Phys. Rev. Res.* **2** 43019
[33] Coleman P and Andrei N 1989 *J. Phys.: Condens. Matter* **1** 4057
[34] Proust C and Taillefer L 2019 *Annu. Rev. Condens. Matter Phys.* **10** 409
[35] Shishido H, Settai R, Harima H and Ōnuki Y 2005 *J. Phys. Soc. Japan* **74** 1103
[36] Friedemann S, Oeschler N, Wirth S, Krellner C, Geibel C, Steglich F, Paschen S, Kirchner S and Si Q 2010 *Proc. Natl Acad. Sci.* **107** 14547
[37] Chang Y Y, Paschen S and Chung C H 2018 *Phys. Rev.* B **97** 035156
[38] Chang Y Y, Hsu F, Kirchner S, Mou C Y, Lee T K and Chung C H 2019 *Phys. Rev.* B **99** 94513
[39] Zhang Y-H and Sachdev S 2020 *Phys. Rev. Res.* **2** 023172
[40] Chen S D *et al* 2019 *Science* **366** 1099
[41] Michon B *et al* 2019 *Nature* **567** 218
[42] Takagi H, Verret S, Doiron-Leyraud N and Marcenat C 2022 *Annu. Rev. Condens. Matter Phys.* **13** 239
[43] Koltenbah B E C and Joynt R 1997 *Rep. Prog. Phys.* **60** 23
[44] Ogata M and Fukuyama H 2008 *Rep. Prog. Phys.* **71** 036501
[45] Hur K L and Maurice Rice T 2009 *Ann. Phys., NY* **324** 1452
[46] Moon E G and Sachdev S 2011 *Phys. Rev.* B **83** 224508
[47] Punk M, Allais A and Sachdev S 2015 *Proc. Natl Acad. Sci.* **112** 9552
[48] Coleman P 1984 *Phys. Rev.* B **29** 3035
[49] Kotliar G and Liu J 1988 *Phys. Rev.* B **38** 5142
[50] Senthil T, Sachdev S and Vojta M 2003 *Phys. Rev. Lett.* **90** 216403
[51] Lee S S 2008 *Phys. Rev.* B **78** 085129
[52] Hermele M, Senthil T, Fisher M P A, Lee P A, Nagaosa N and Wen X-G 2004 *Phys. Rev.* B **70** 214437
[53] Wang J, Chang Y-Y and Chung C-H 2022 *Proc. Natl Acad. Sci.* **119** e2116980119
[54] Berg E, Fradkin E, Kivelson S A and Tranquada J M 2009 *New J. Phys.* **11** 115004
[55] Dai Z, Zhang Y H, Senthil T and Lee P A 2018 *Phys. Rev.* B **97** 174511
[56] Sato Y *et al* 2017 *Nat. Phys.* **13** 1074
[57] Cava R J, van Dover R B, Batlogg B and Rietman E A 1987 *Phys. Rev. Lett.* **58** 408
[58] Cava R J, Batlogg B, van Dover R B, Murphy D W, Sunshine S, Siegrist T, Remeika J P, Rietman E A, Zahurak S and Espinosa G P 1987 *Phys. Rev. Lett.* **58** 1676
[59] Martin S, Fiory A T, Fleming R M, Schneemeyer L F and Waszczak J V 1990 *Phys. Rev.* B **41** 846
[60] Hussey N E, Cooper R A, Xu X, Wang Y, Mouzopoulou I, Vignolle B and Proust C 2011 *Phil. Trans. R. Soc.* A **369** 1626
[61] Rourke P M C, Bangura A F, Benseman T M, Matusiak M, Cooper J R, Carrington A and Hussey N E 2010 *New J. Phys.* **12** 105009
[62] Li X, Kono J, Si Q and Paschen S 2023 *Front. Electron. Mater.* **2** 1–12
[63] Valla T, Fedorov A V, Johnson P D, Wells B O, Hulbert S L, Li Q, Gu G D and Koshizuka N 1999 *Science* **285** 2110
[64] Abrahams E and Varma C M 2000 *Proc. Natl Acad. Sci.* **97** 5714
[65] Kaminski A *et al* 2000 *Phys. Rev. Lett.* **84** 1788
[66] Varma C M, Littlewood P B, Schmitt-Rink S, Abrahams E and Ruckenstein A E 1989 *Phys. Rev. Lett.* **63** 1996
[67] Varma C M 2020 *Rev. Mod. Phys.* **92** 031001
[68] Horio M *et al* 2018 *Phys. Rev. Lett.* **121** 077004
[69] Zhong Y, Chen Z, Chen S-D, Xu K-J, Hashimoto M, He Y, Uchida S I, Lu D, Mo S-K and Shen Z-X 2022 *Proc. Natl Acad. Sci.* **119** e2204630119
[70] Ioffe L B and Larkin A I 1989 *Phys. Rev.* B **39** 8988
[71] Wang X and Chowdhury D 2023 *Phys. Rev.* B **107** 125157
[72] Cooper R A *et al* 2009 *Science* **323** 603
[73] Parcollet O, Georges A, Kotliar G and Sengupta A 1998 *Phys. Rev.* B **58** 3794
[74] Georges A and Mravlje J 2021 *Phys. Rev. Res.* **3** 43132
[75] Ataei A *et al* 2022 *Nat. Phys.* **18** 1420
[76] Badoux S *et al* 2016 *Nature* **531** 210

[77] Collignon C *et al* 2017 *Phys. Rev.* B **95** 224517
[78] Kanigel A, Chatterjee U, Randeria M, Norman M R, Koren G, Kadowaki K and Campuzano J C 2008 *Phys. Rev. Lett.* **101** 137002
[79] Niu J *et al* 2024 Equivalence of pseudogap and pairing energy in a cuprate high-temperature superconductor (arXiv:2409.15928 [cond-mat.supr-con])
[80] Lee P A 2014 *Phys. Rev.* X **4** 031017
[81] Sobota J A, He Y and Shen Z-X 2021 *Rev. Mod. Phys.* **93** 025006
[82] Emery V J and Kivelson S A 1995 *Nature* **374** 434
[83] Kondo T, Hamaya Y, Palczewski A D, Takeuchi T, Wen J S, Xu Z J, Gu G, Schmalian J and Kaminski A 2011 *Nat. Phys.* **7** 21
[84] Chung C H, Marston J B and McKenzie R H 2001 *J. Phys.: Condens. Matter* **13** 5159
[85] Cancrini N, Caprara S, Castellani C, Castro C D, Grilli M and Raimondi R 1991 *Europhys. Lett.* **14** 597
[86] Paul I, Pépin C and Norman M R 2007 *Phys. Rev. Lett.* **98** 026402
[87] Nguyen K V, Chang Y-Y, Remund K and Chung C-H 2025 (unpublished)
[88] Anderson P W 1987 *Science* **235** 1196
[89] Chien T R, Wang Z Z and Ong N P 1991 *Phys. Rev. Lett.* **67** 2088
[90] Harris J M, Yan Y F and Ong N P 1992 *Phys. Rev.* B **46** 14293
[91] Carrington A, Mackenzie A P, Lin C T and Cooper J R 1992 *Phys. Rev. Lett.* **69** 2855
[92] Jaoui A, Das I, Di Battista G, Díez-Mérida J, Lu X, Watanabe K, Taniguchi T, Ishizuka H, Levitov L and Efetov D K 2022 *Nat. Phys.* **18** 633
[93] Lee K *et al* 2023 *Nature* **619** 288
[94] Song Z D and Bernevig B A 2022 *Phys. Rev. Lett.* **129** 047601
[95] Chou Y-Z and Das Sarma S 2023 *Phys. Rev. Lett.* **131** 026501
[96] Hu H, Bernevig B A and Tsvelik A M 2023 *Phys. Rev. Lett.* **131** 026502
[97] Zhou G-D, Wang Y-J, Tong N and Song Z-D 2024 *Phys. Rev.* B **109** 045419
[98] Hepting M *et al* 2020 *Nat. Mater.* **19** 381